AIChE

A Novel, Structure-Tracking Monte Carlo Algorithm for Spray Fluidized Bed Agglomeration

Mathias Dernedde, Mirko Peglow, and Evangelos Tsotsas
Thermal Process Engineering, Otto-von-Guericke University, 39106 Magdeburg, Germany

DOI 10.1002/aic.13709
Published online December 12, 2011 in Wiley Online Library (wileyonlinelibrary.com).

A stochastic modeling approach to fluidized bed agglomeration is presented. First, the fundamentals of a general Monte Carlo algorithm are discussed, namely the correlation of real with simulation time and the size of the simulation box. Two different approaches regarding the morphological description of particle structure development are then compared for different theoretical test cases. The first approach (concept of positions) is a fast and effective geometrical discretization to follow properties such as primary particle number per agglomerate throughout the simulation. The second approach is a new three-dimensional (3-D) structure algorithm, which allows a complete, unrestricted description of the spatial evolution of particles related to physical microprocesses. The 3-D algorithm enables to apply distributed particle and droplet sizes, which is not possible in the concept of positions. In the perspective, the structural growth of particles can be connected to process conditions, opening new possibilities for process and product design. © 2011 American Institute of Chemical Engineers *AIChE J,* 58: 3016–3029, 2012
Keywords: fluidized bed, agglomeration, stochastic modeling, Monte Carlo method

Introduction

The mathematical description of particulate processes is often done by the continuous population balance equation (PBE).[1] Its terms account for growth, breakage, aggregation, and nucleation within the dispersed phase. The PBE can be multidimensional and delivers the temporal evolution of the density distribution of certain particle properties such as size or binder mass. Applications range from crystallization to polymerization, precipitation, or agglomeration. The latter can be performed in mixers, drums or fluidized beds. Fluidized beds combine binder addition and drying in a single apparatus and are, thus, advantageous for many applications in food, detergent, or pharmaceutical industries. Fluidized bed spray agglomeration is based on the cluster-like coalescence of primary particles by means of solidifying, viscous binder bridges which are created by random collisions with other particles. Agglomeration processes mainly aim at enlarging dusty powders or integrating various liquid or particulate components in a single compound structure.[2] The resulting products are porous solids of relatively low density. Compared to the starting material, they are easier to handle during transportation and redisperse for use.

The population balance can be solved in different ways. The traditional approach requires discretization of the chosen property coordinate(s) and solves the integro-differential PBE[3] numerically in time. The discretization is cumbersome as the shape of the property distribution and its dynamic change should be known in advance.[4] Furthermore, the PBE contains macroscopic kinetics that need to be validated experimentally and can only represent a certain apparatus under specific process conditions (i.e. apparatus, material system). This article presents an alternative stochastic solution of the population dynamics. As proposed by other authors,[4–7] the Monte Carlo method seems to be highly appropriate, due to the discrete nature of the process. Instead of considering agglomeration to be continuous, macroscopic, and deterministic, the process is understood as a sequence of random events. Instead of taking into account the complete population, a discrete sample is chosen, representing the distributed properties of the whole population. Common classifications of different Monte Carlo methods are given in Table 1. Detailed descriptions are given in the cited literature.

In this article, an event-driven, constant-number Direct Simulation Monte Carlo method is presented. To this purpose, the fluidized bed is considered as a homogeneous and well-mixed system. The influence of external, spatial coordinates is not taken into account. Such an influence can arise from the spray jet, and it may be described by discrete particle simulations[12] or by compartment models. Compartment models typically distinguish between a spraying and a drying zone, with the possibility of adding further spatial domains (such as an inactive zone, i.e. in Maronga and Wnukowski[13]). The Monte Carlo approach can be extended to compartments operated under different conditions, but exchanging particles with each other. However, this extension shall be the topic of future work. At present, the focus is on one single compartment—a situation which is not unrealistic for small fluidized beds with intensive spraying.

Based on the morphological particle description of Terrazas-Velarde et al.,[5,14,15] denoted by "concept of positions" (CoP), their algorithm is extended to retrieve additional

Correspondence concerning this article should be addressed to M. Dernedde at mathias.dernedde@ovgu.de.

Table 1. Common Classification of Monte Carlo Methods

Feature	Option I	Option II
Regulation of simulation box size	Constant number[4]	Constant volume[6]
Progress in time	Event-driven[8]	Time-driven[9]
Motion of particles	Trajectory method[10]	Direct Simulation[11]

information about droplet efficiency and particle structure. Additionally, a novel 3-dimensional structure algorithm that takes into account the unrestricted spatial development of agglomerates is introduced. The two algorithms are compared for different theoretical test cases, and the correctness of their results is checked by analytical solutions. The discussion will start by introducing key features of the two Monte Carlo algorithms: the correlation of simulation with real time and the dynamic regulation of the simulation box size. The expressions "particle", "aggregate", or "agglomerate" are considered synonymous for particle clusters, whereas "primary particle" denotes the initial single particle in the powder bed.

Monte Carlo Algorithm

Scaling and regulation

The simulation box represents a sample of the solid hold up in the real fluidized bed container. In this simulation box, particles interact physically in the same way as they do in the real system. Although properties are the same for both, model and process system, absolute values need to be transformed by a scaling factor S

$$S = \frac{N_{\mathrm{pp,MC}}}{N_{\mathrm{pp}}} \tag{1}$$

The primary particle number of the (batch) process N_{pp} will remain constant. However, only the number of entities will remain constant in the simulation box (Figure 1). This means that in systems dominated by aggregation—two or more particles form a new particle—one will need to replace coagulated particles by copying to retain a high level of statistical accuracy. This causes an increase of primary particle number in the simulation box. For breakage-dominated systems—one particle breaks in various fragments—the opposite case is relevant: selected, newly born particles need to be deleted.

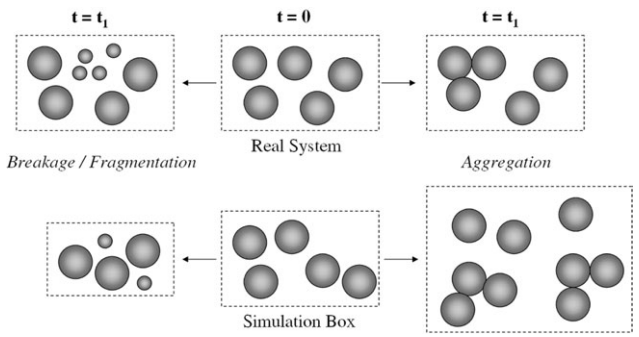

Figure 1. The particle number changes by aggregation (right-hand side) or breakage (left-hand side) in real particle systems.

To maintain the statistical accuracy of the representative simulation box, particles are randomly copied or deleted. Consequently, the simulated volume will either increase (aggregation) or decrease (breakage) with time.

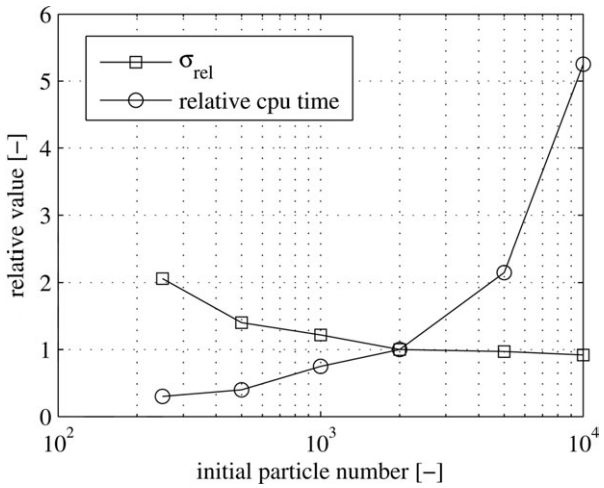

Figure 2. Dependence of simulation accuracy and speed on the initial particle number in the simulation box according to Terrazas-Velarde et al.[5]

The standard deviation and CPU time of a simulation with 2000 particles were used as reference values.

Simulation box size

The general idea of the direct simulation Monte Carlo algorithm is that a relatively small number of computational particles can represent all the properties of the real system. The number of particles in the simulation box is a compromise between short computational time and high confidence level of the calculation. In event-driven Monte Carlo methods, the time step is correlated to the time elapsed between two consecutive events, which can be either an interparticle collision or the addition of a binder droplet to the system. Generally applies: the shorter the time step, the higher is the statistical accuracy. As described in the following section, more particles in the simulation box will lead to a decrease in the time step and an improvement of accuracy.

Zhao et al.[16] compared four different Monte Carlo methods regarding the initial particle number in the simulation box. They found that every method delivers satisfactory results with a particle number of 1000 with computational times in the order of 10^2 to 10^3 s. Usually, the particle number to be simulated on a desktop computer ranges from 10^3 to 10^5 particles.[6,11] Terrazas-Velarde et al.[5] tested the effect of different primary particle numbers from 250 up to 10,000 particles on the simulation speed and the accuracy of the simulation under otherwise identical conditions (Figure 2). They report growing deviations of the mean particle size as a function of time for particle numbers below 1000, but no further improvement of the values above 2000 particles. On the basis of these results, we will use 1000 particles to initially fill the simulation box in the present study.

Event frequency and selection of time step

In this study, we are presenting a Kinetic Monte Carlo method to correlate the simulation box process with real time. The method assumes that all relevant time constants of the process are known. In chemical reaction engineering, these time constants are called "reaction rates," whereas in our stochastic formulation of the process model, the time

constants can be understood as "probability per unit time" that the specific event is going to happen.[17] Corresponding to the events "droplet addition" and "interparticle collision," two event frequencies can be defined.

The droplet addition frequency is trivial and can be directly adapted from the real system. The volume flow rate of binder through the atomizer is a given process parameter. By assuming an average volume of the created single droplets, one can derive the number flow of droplets per unit time $\dot{N}_{\mathrm{drop}}$. To scale the droplet addition rate in such a way that it fits the simulation box, we need to multiply the real droplet addition rate with the scaling factor S

$$f_{\mathrm{wet,MC}} = \dot{N}_{\mathrm{drop}}\, S \tag{2}$$

The frequency of collisions between particles is much less intuitive to identify. Few attempts to measure or simulate it can be found in literature. Buffiere and Moletta[18] used a high-frequency response hydrophone to measure the collision frequency in an inverse three-phase fluidized bed. They obtained an empirical correlation that delivers high values in the order of 10^2 to 10^4 collisions per particle and second. This seems to be contradictory to other results, because thermal effects such as the drying of deposited droplets (or their penetration in porous substrates) would completely lose their relevance for the process at such high collision frequencies. Assuming that a particle collides 1000 times per second, a wet spot on the surface would be hit anyway, no matter if the droplet vanishes after 0.1 s (high temperature) or 10 s (very low temperature). However, the importance of thermal parameters, such as the operating temperature, has been repeatedly demonstrated by experiments (see, e.g., Terrazas-Velarde et al.[15]). Another approach is the model of Oesterle and Petitjean.[19] They used a trajectory method to simulate the collision rate in a nondilute gas-solid flow. In analogy with the kinetic theory of gases, they derived an analytic equation and tested it for convective particle transport in a horizontal pipe under different solid loading rates. This stochastic collision model delivers collision frequencies in the order of 10^0 to 10^2 collisions per particle and second, which seems to be more applicable to fluidized beds. In the present study, a constant collision frequency of $f_{\mathrm{coll}} = 2$ collisions per particle and second was assumed. Multiplied by the number of particles in the simulation box, the total value for the collision frequency becomes

$$f_{\mathrm{coll,MC}} = \frac{1}{2} f_{\mathrm{coll}}\, N_{\mathrm{p,MC}} \tag{3}$$

The prefactor 1/2 results from the consideration of only binary collisions.

Within the kinetic Monte Carlo algorithm, the system jumps from one state to another.[20] To leave a certain state, the system has two possible escape options: addition of another droplet or collision between two particles. In contrast to the deterministic approach of continuous development in time, the stochastic procedure resembles a stairway. While residing in one state, the system loses its memory of the past. Thus, in every moment of time, the system can find the way out of the actual state. The probability of the system leaving the actual state P within a small time interval Δt is simply the frequency of the state jump f_{event} multiplied by the time step. For a very large number of time intervals, the probability of the system leaving the actual state is

$$P = 1 - \exp(-f_{\mathrm{event}}\Delta t) \tag{4}$$

The density function of this cumulative distribution (time derivative of P) is

$$p = f_{\mathrm{event}} \exp(-f_{\mathrm{event}}\Delta t) \tag{5}$$

Therefore, the probability to leave one state and the state to which the system is going to jump in next are defined by its frequency or rate—as the length of time between two consecutive states. Following Gillespie's "Inversion Method,"[17] one can generate the exponential waiting time by inverting Eq. 4 with $P = r_1$ and replacing $1 - r_1$ by the statistically equivalent random variable r_1

$$t_{\mathrm{step}} = -\frac{1}{f_{\mathrm{event}}}\, \ln(r_1) \tag{6}$$

where r_1 is a uniformly distributed random number, $r_1 \in]0, 1]$. Figure 4 shows the derivation of an exponentially weighted time step according to Eq. 6. To extend this algorithm to a more complex network of possible events,[17] the single event frequencies are added up to

$$f_{\mathrm{tot,MC}} = f_{\mathrm{coll,MC}} + f_{\mathrm{wet,MC}} \tag{7}$$

The discrete time step between two events is now

$$t_{\mathrm{step}} = -\frac{1}{f_{\mathrm{tot,MC}}} \ln(r_1) \tag{8}$$

Averaging a statistically sufficient number of single time steps will lead to $t_{\mathrm{step}} = 1/f_{\mathrm{tot,MC}}$. Using a constant step size $1/f_{\mathrm{tot,MC}}$ might be simpler but would neglect the stochastic nature of the process and the Markovian characteristic of memoryless inter-event time. The exponential distribution is used whenever events may occur after random waiting times, such as radioactive decay or incoming flights on an airport.

In Figure 3, the distributed total process time is compared to the expected analytic value to visualize the possible time range of our stochastic procedure. A process consisting of 10^4 events, which corresponds to around 10 s of process time, was considered and the simulation was repeated 100 times with the same set of parameters. The analytic process time is then simply

$$t_{\mathrm{analytic}} = -\frac{1}{f_{\mathrm{tot,MC}}} N_{\mathrm{event}} \tag{9}$$

with the time step at a constant value of $1/f_{\mathrm{tot,MC}}$ instead of being exponentially distributed (Eq. 8). The total time length of one simulation run can deviate by more than 2% compared to the analytic process time. It is in the nature of stochastic simulations that only mean values are reproducible. While deterministic, macroscopic models with constant time steps give a first-order approximation of the process, stochastic simulations have variable time steps that sum up to the process time. The stochastic solution is exact for a single scenario which can occur with a certain probability. Depicted in Figure 3, the mean process time of all 100 simulation runs deviates by only 0.39% from the expected value.

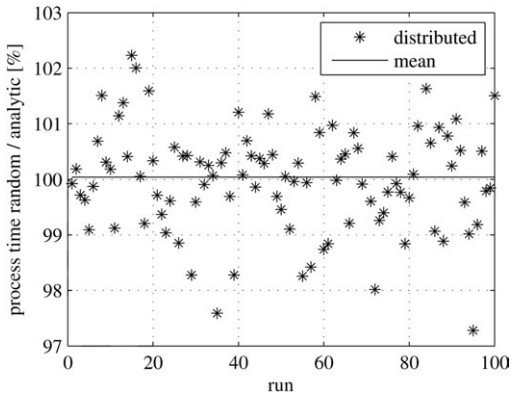

Figure 3. Total process times of 100 single simulation runs under equal conditions.

The mean value of all simulations agrees well with the expected, analytically calculated process time. However, single simulations deviate by more than 2%, which is in the nature of stochastic processes.

In our random-walk process, the collision frequency $f_{\mathrm{coll,MC}}$ is around 100 times larger than the droplet addition rate $f_{\mathrm{wet,MC}}$. This means that a collision between two particles is 100 times more likely to occur than the addition of a droplet. Thus, the collision frequency is the highest reaction rate in the system and scales the discretization of process time and CPU time. Real time steps become very short when the collision frequency increases.

Terrazas-Velarde et al.[5] follow a different approach. In their constant-volume Monte Carlo method, the time step is constant and defined only by the collision frequency (Figure 4)

$$t^{*}_{\mathrm{step}} = \frac{1}{f_{\mathrm{coll}}} \tag{10}$$

All particles are separated in two groups, which collide during one time step. A droplet is added when the process reaches the droplet addition time. This formulation of the algorithm is less intuitive as time steps are quite large and the system freezes until every single particle has collided with a collision partner. Considering every binary collision to be an aggregation event, one can easily derive the continuous decrease of total particle number in the system from

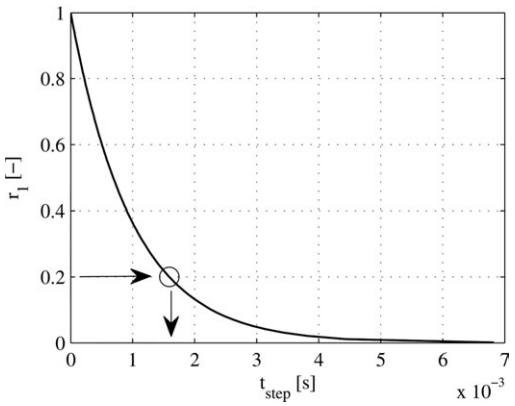

Figure 4. Example for the selection of waiting time t_{step} (time interval between two subsequent system states) with the help of a random number r_1 and an exponential distribution (r_1 = 0.2, t_{step} = 0.0016 s).

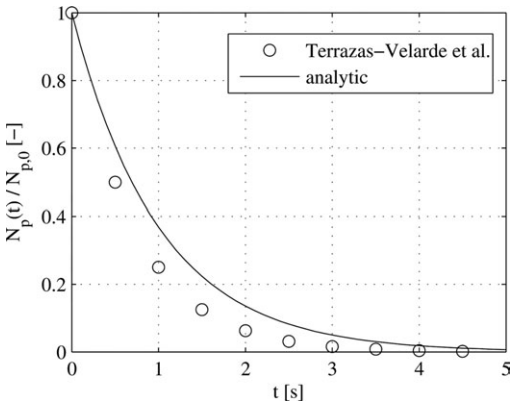

Figure 5. Assuming the ratio between collisions and aggregations to be unity, one can derive the decrease of particle number analytically.

For a collision frequency of $f_{\mathrm{coll}} = 2$, the model of Terrazas-Velarde et al.[5] deviates from this solution by not taking into account the number decrease during every collision step.

$$\frac{dN_{\mathrm{p}}}{dt} = -\frac{f_{\mathrm{coll}}}{2} N_{\mathrm{p}} \tag{11}$$

to the analytical solution

$$\frac{N_{\mathrm{p}}}{N_{\mathrm{p,0}}} = \exp\left(-\frac{f_{\mathrm{coll}}}{2} t\right) \tag{12}$$

Figure 5 shows a disadvantage of the model of Terrazas-Velarde et al.[5] In the present constant-number Monte Carlo method, the absolute collision frequency $f_{\mathrm{coll,MC}}$ is exact because the number of aggregates in the simulation box $N_{\mathrm{p,MC}}$ is kept constant throughout the simulation (see Eq. 3). Terrazas-Velarde et al. keep, however, the value of the collision frequency constant throughout a series of aggregations, until every simulation particle has experienced one collision. Only when the simulated population reaches half or double of the initial number, a regulation procedure will adjust the number of primary particles. This may result in a significant deviation compared to the analytical solution. The described effect loses its importance when aggregation rates below 1% are applied to the system and number decrease per collision event is less frequent.

Selection of events

While the process time is advanced by t_{step}, it is necessary to draw a second random number $r_2 \in [0,1]$ to select which event is going to happen next

$$\text{collision}: \; f_{\mathrm{tot,MC}} r_2 \leq f_{\mathrm{coll,MC}} \tag{13}$$

$$\text{droplet addition}: \; f_{\mathrm{coll,MC}} < f_{\mathrm{tot,MC}}\, r_2 \leq f_{\mathrm{tot,MC}} \tag{14}$$

This method is computationally efficient, as only two random numbers need to be drawn per time step. The system is guaranteed to evolve to another state in every iteration step without any rejections.[20]

Description of Particle Morphology

Extended Concept of Positions

The structure of a particle has great influence on its functionality, for example on the release of active ingredients in

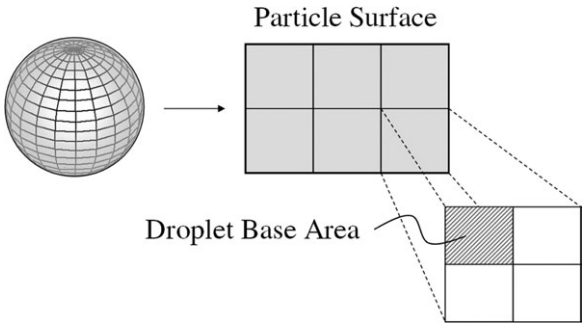

Figure 6. The CoP of Terrazas-Velarde et al.[5] divides the particle in $K_{max} = 6$ sectors.

Every sector contains an integer number of droplet positions, either wet or dry. Four droplet positions per sector were chosen for the present illustration.

pharmaceutical or agricultural applications. In the considered agglomeration processes, particles are joined together by collisions. However, the collision between two particles does not necessarily lead to a desired aggregation event. To this purpose, two conditions must be fulfilled: first, a liquid film must be present at the contact point of either one or both colliding particles. Second, the kinetic energy of impact needs to be dissipated by the liquid film. The latter is described as the Stokes criterion[21] and will not be considered in this study. Stepanek et al.[22] combined the Stokes criterion with the spatial distribution of binder in wet granules to describe the kinetics of the process by a coalescence kernel. Their granules consisted of nonspherical primary particles, which had been arranged in dense structures, assuming equilibrium state (no drying and no shrinkage of droplets). The structure was simulated as a Gaussian Blob using the Volume of Fluid method.

Terrazas-Velarde et al.[5] introduced the CoP to model the particle structure in their Monte Carlo approach to fluidized bed agglomeration. Assuming a maximum coordination number $K_{max} = 6$, the particle surface was partitioned to an equal number of K_{max} sectors. The area of every sector was subdivided to hold an equal, integer number of deposited droplets. The total number of droplet positions on a primary particle can be written as

$$N_{pos,tot} = \frac{d_{pp}^2}{a_{drop}^2} \tag{15}$$

where d_{pp} is the primary particle diameter and a_{drop} is the base radius of a deposited droplet. The number of positions per sector is as follows

$$N_{pos,sec} = \frac{N_{pos,tot}}{K_{max}}, \quad N_{pos,sec} \in N \tag{16}$$

As $N_{pos,sec}$ is a discrete measure, it is rounded to the nearest integer value. The positions are encoded in a binary code as either dry (0) or wet (1), meaning the absence or presence of a droplet. From the position matrices of both colliding particles, one position per particle is randomly chosen for collision. At least one of both positions needs to be wet for an aggregation to occur. The geometrical discretization of a primary particle following this method is displayed in Figure 6.

The following sections of this article will be mainly devoted to the new 3-D structure model of aggregates. However to compare sterical effects, such as the impediment of droplets, created by the morphological model approach itself, we have also extended the CoP. In this way, more information about the particle structure can be extracted. The extended CoP labels the positions on a particle to one out of seven possible groups, as summarized in Table 2. Two independent attributes are considered to this purpose. First, the position can be either blocked or sterically accessible for other colliding particles or droplets. Second, the position may contain a droplet which is still wet or already dried. Primary particles preserve all their positions when they are integrated in an agglomerate. As soon as a binder bridge is formed between two particles, the entire sector holding the colliding position is considered to be blocked for further collisions with other particles or droplets. This means that all droplet positions within this sector are deactivated, even those not actually involved in bridge formation with another particle. The consequence is a dynamic deactivation of droplets not only by drying and bridge formation but also by sterical hinderance.

The collision algorithm works as follows, using the labels described in Table 2:

1. Choose two agglomerates randomly for binary collision.
2. Choose one position per agglomerate for this collision.
3. Check whether one or both positions are labeled as 2 or not.
4. If yes (at least one position is labeled as 2 and, thus, contains a wet droplet): label all other positions within these two sectors as 3, 4, or 7, according to their previous occupation. The two colliding positions are labeled as 5.
5. If no (both positions are empty, meaning labeled as 1, or sterically hidden): choose new positions and check the labels again.

The deposition of droplets works similarly. It should be noted, that a droplet can only be placed at an empty position (label 1). The new label is then 2: the position contains a droplet and is not sterically hidden for collision. Droplet deposition on already wet positions is not foreseen in the extended CoP.

Interparticle collisions in three dimensions

In the following, we will explain the new 3-D structure algorithm which allows a free dynamic development of particle morphology during the simulated agglomeration process.

If during the random walk from one system state to another the event ''collision'' is chosen to be next, two particles A and B are randomly selected from the simulation

Table 2. Possible Labels Used in the Extended CoP: Positions can be Accessible for Collision or Droplet Deposition, or Sterically Hidden[*]

Label	Sterical accessibility	Presence of droplet	Droplet state
1	+	−	No droplet
2	+	+	Wet
3	−	−	No droplet
4	−	+	Wet
5	−	+	Binder bridge
6	+	+	Dry
7	−	+	Dry

[*]Independently, the position can hold a wet or dry droplet, or it can be empty.

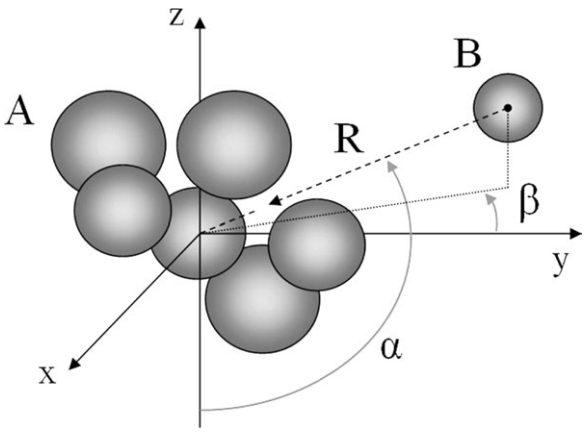

Figure 7. Procedure for binary collision of particles.

Collision partner *B* is shifted into the local coordinate system of *A*. The center point of *B* is placed in collision direction *R*, which is defined by the vertical angle α and the horizontal angle β.

box. Every particle is described by a local coordinate system placed at the center of the original (initial) primary particle. Primary particles are assumed to be perfect spheres so that they can be geometrically described by their center point coordinates and their radius r_p.

First, the collision direction pointing toward the coordinate origin is expressed by two angles, $\alpha \in [0, \pi]$ and $\beta \in [0, 2\pi)$. These angles are selected by drawing two uniform random numbers r_α, $r_\beta \in [0,1]$ to

$$\alpha = \cos^{-1}(2r_\alpha - 1) \tag{17}$$

$$\beta = 2\pi r_\beta \tag{18}$$

α and β are spherical coordinates of points uniformly distributed over the surface of a unit sphere. They can be used to obtain the Cartesian coordinates of the collision vector R in x-, y-, and z-direction

$$R_x = \sin\alpha\cos\beta \tag{19}$$

$$R_y = \sin\alpha\sin\beta \tag{20}$$

$$R_z = \cos\alpha \tag{21}$$

While the first collision partner A remains static in its coordinate system, the collision partner B is also transferred into the coordinate system of A. The center point of B's original primary particle is placed on the collision direction R in a distance of twice the sum of the outer radii of the two particles, so that A and B do not yet touch each other. All other particle and droplet coordinates of B are shifted accordingly. There is no slip, rotation or reconstitution of particles. Consequently, the spatial structure of every particle is maintained during collisions. The collision procedure is depicted in Figure 7, where B is chosen to be a primary particle for the sake of simplicity. In reality, the algorithm also works with arbitrarily complex aggregates.

To find the primary particles of A and B between which the bridge will be formed, we use the collision direction. From the center point of every ith primary particle of B, we draw R_i by parallel translation and calculate the distance $D_{i,j}$ between R_i and the center point of the jth primary particle of A (Figure 8). If $D_{i,j}$ is smaller than or equal to the sum of the primary particle radii $r_i + r_j$, the primary particles i and j will contact each other. In this way, the algorithm narrows the potential number of contacting primary particles. Next, we need to know which specific primary particle of A will be the outer particle to be touched first when moving B in collision direction. This is achieved by defining and minimizing a parameter λ in the expression for the geometrical translation Δ_i of every primary particle of B

$$\Delta_i = \lambda_i \begin{pmatrix} R_x \\ R_y \\ R_z \end{pmatrix} + \begin{pmatrix} x_{M,i} \\ y_{M,i} \\ z_{M,i} \end{pmatrix} \tag{22}$$

Here, $x_{M,i}$, $y_{M,i}$, and $z_{M,i}$ are the center point coordinates of every primary particle of B. λ_i is first calculated for every combination of i and j that fulfills the condition $D_{i,j} \leq r_i + r_j$. From the resulting set of λ_i we then identify the minimum value, which gives us the combination of two primary particles i and j that will directly contact each other. In this way, an overlap of primary particles, which would be physically unreasonable as our particles are considered to be rigid and perfectly spherical, is excluded.

Now it is possible to determine the contact point between the two primary particles. Going back to our initial statement, two conditions have to be fulfilled for successful aggregation: a liquid film must be, first, present and, second, able to dissipate the kinetic energy of impact. The second condition is usually comprised in the Stokes criterion, which will not be considered here. Thus, we only have to decide whether a collision is wet or not to identify aggregation in the algorithm. Therefore, the wetted area of the particle (see Figure 9)

$$A_{p,wet} = 2\pi x_h r_{pp} \tag{23}$$

is set equal to the droplet base area

$$A_{drop} = \pi a_{drop}^2 \tag{24}$$

to obtain the lateral height of the wetted surface of the particle

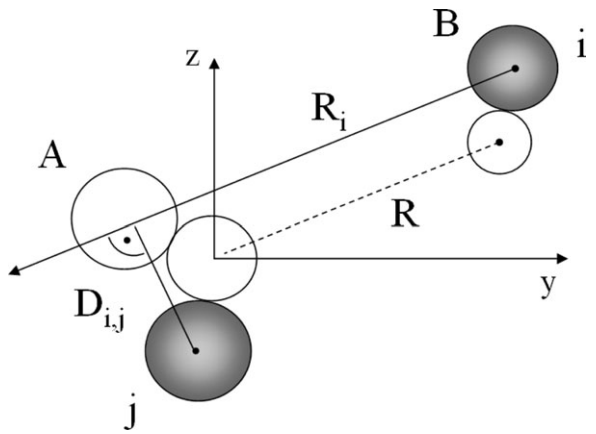

Figure 8. 2-D illustration of the algorithm to find the set of possible contact points of two colliding particles.

The distance $D_{i,j}$ between R_i and the center of primary particles j in A is checked. If $D_{i,j} \leq r_i + r_j$, bridge formation between primary particles i and j is possible. Additionally, it must be checked which primary particle of A is the first one to be contacted when B is moved toward A on R.

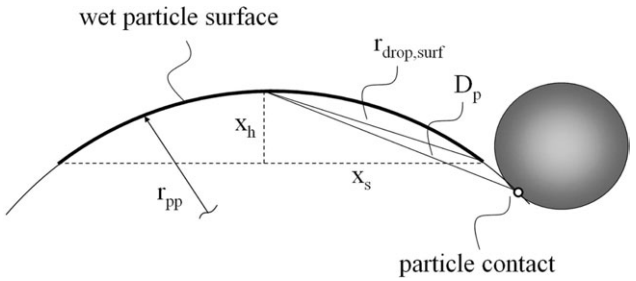

Figure 9. To check whether a collision was wet or dry, the distance between the contact point of two particles and the droplet center D_p is compared to the dimension of the droplet base area on the particle surface $r_{drop,surf}$.

The depicted situation would be considered as dry collision.

$$x_h = \frac{a_{drop}^2}{2r_{pp}} \tag{25}$$

With

$$x_s = \sqrt{r_{pp}^2 - \left(r_{pp} - x_h\right)^2} \tag{26}$$

we can calculate the distance between the center point of the deposited droplet to the edge of the droplet base area $r_{drop,surf}$. Although the curvature of the particle surface is neglected, the percental surface coverage by a deposited droplet is preserved. This is important for obtaining the correct probability of a colliding particle to hit a wet spot on the collision partner and successfully aggregate, compare with the discussion in the Results of this article. The criterion to decide whether a collision was wet is

$$r_{drop,surf} = \sqrt{x_h^2 + x_s^2} \geq D_p \tag{27}$$

D_p is the distance between particle contact and center point of the droplet. If the particle contact is within the droplet base area, the collision is considered to be wet: particles will stick together held by a liquid binder bridge. The geometrical situation is depicted in Figure 9. The criterion is checked for both colliding particles as either can have a wet surface area at the collision spot. If this is the case, every primary particle, droplet and binder bridge of B is shifted by $\Delta_{min}(\lambda_{min})$. Particles A and B form a new agglomerate with updated properties. To keep the total particle number in the simulation box constant, the vacancy of former B needs to be filled by randomly selecting and doubling another particle from the simulation box. If the collision was dry, colliding particle B will remain independent and it will be transferred back to its own local coordinate system.

It should be stressed that the selection of the particle to be copied after a successful aggregation is random, but the structure of this particle is not, because the structure of every particle in the simulation box depends on the entire previous history of the process. In the full version of the simulation, droplet aging by drying or penetration and the fulfillment of the Stokes criterion will be part of this history, depending on process conditions. Consequently, the evolution of properties and agglomerate structure is specific to material and process parameters in the simulation box. Therefore, particle structure is not randomized by copying, and all previous information is preserved during any agglomeration event.

Without a doubt, the proposed collision algorithm is numerically expensive. Every primary particle position involved needs to be checked in relation to all other primary particles. Especially for growing primary particle numbers per aggregate, simulation time rises. To tackle this problem, Leba et al.[23] presented a more efficient cluster-cluster-algorithm. A drawback of their method is that primary particles need to be monodisperse, whereas the present algorithm is able to build up structures from polydisperse primary particles. Furthermore, we have to take into account that collisions can be either wet or dry. This essential physical information cannot be obtained from the algorithm of Leba et al.

Collisions between particles and droplets

To calculate the droplet base radius a_{drop}, the curvature of the particle surface is neglected, assuming a planar substrate. Deposited droplets are then semielliptical. They are characterized by their center point coordinates and the length of their half-axes, namely a_{drop} and h_{drop}, which is the central height of the droplet. The center point of a deposited droplet sits on the surface of a particle. In our case, we use a particle diameter of $d_p = 200\mu m$ and a free (spherical) droplet diameter of $d_{drop} = 40\mu m$. As the free droplet volume V_{drop} is a given process parameter, the dimensions after spreading[24] can be calculated to

$$a_{drop} = \left(\frac{3V_{drop}}{\pi}\frac{\sin^3\vartheta}{2 - 3\cos\vartheta + \cos^3\vartheta}\right)^{\frac{1}{3}} \tag{28}$$

$$h_{drop} = a_{drop}\left(\frac{1 - \cos\vartheta}{\sin\vartheta}\right) \tag{29}$$

where ϑ is the contact angle. A value of $\vartheta = 40^\circ$ applies for a 6 wt-% solution of the here considered binder material hydroxyl-propyl-methyl-cellulose in water, deposited on nonporous glass particles.

The collision algorithm for droplets is analogous to the previously described particle-particle collision algorithm. Compared to the CoP[15] droplet volumes can vary. Overlapping of droplets is possible, as there are no strictly defined positions on the particle surface. In this study, we assume monodisperse droplets. Droplet predrying is switched off in the algorithm so that every added droplet will be immediately deposited on a randomly selected simulation particle.

Results and Discussion

Model verification

To verify its theoretical correctness, we will apply the 3-D agglomeration model for different test cases and compare results with the extended CoP (Table 4). For the sake of a systematic approach to this comparison, we will not take into account the following:

- The predrying of droplets after leaving the atomizer.
- The drying of deposited droplets on the particle surface or their penetration in porous particles.
- The breakage of agglomerates or the attrition of primary particles.

Because of the limited set of considered microprocesses, a direct comparison with experimental results would not be

Table 3. Simulation Parameters of the Base Case

Parameter	Value	Unit
Bed mass, M_{bed}	0.5	kg
Primary particle diameter, d_{pp}	200	μm
Primary particle density, ρ_s	2400	kg/m^3
Binder contact angle, θ	40	$^\circ$
Liquid binder density, ρ_b	1020	kg/m^3
Binder volume flow rate, $\dot{V}_b$	300	ml/h
Binder mass fraction, w_b	6	%
Free droplet diameter, d_{drop}	40	μm
Collision frequency, f_{coll}	2	1/s
Number of particles in the simulation box, N_{MC}	1000	–

reasonable. It should, however, be noticed, that the CoP, which is used as a benchmark and reference, has been shown to appropriately describe measured data.[14,15] Simulation parameters for the base case are listed in Table 3.

Different test cases that will be discussed in the following sections are given in Table 4. Cases A–C are physically not realistic but serve the purpose of theoretical verification and comparison of the two simulation algorithms: the CoP and the novel 3-D structure algorithm. In Case B, every collision is considered to be successful, even a dry-dry collision. On contrary, collisions never lead to bridge formation in Cases A and C, not even collisions on a wet spot. Case D reflects the physically reasonable situation that a binder bridge may be formed if wet binder is present between two colliding particles. As aggregates build up, the sterical accessibility of droplets becomes relevant, which will be discussed in detail.

Case A: one droplet per particle, no aggregation

Rather than dynamically adding the binder liquid, one single droplet is randomly placed on every primary particle in the simulation box at time $t = 0$ in Case A (Figure 10). Furthermore, every collision is considered to be unsuccessful. This means, that no matter if a collision was wet or dry, there will be no aggregation in the simulation box. Droplets will not shrink and will not be impeded by other particles, as no aggregation occurs.

By performing this calculation, we can check the collision efficiency η_{coll}, which should be equivalent to the ratio between droplet base area $A_{drop,base}$ and total particle surface area $A_{p,surf}$. As a binary collision involves two particles, the surface coverage of a single particle needs to be multiplied by a factor of 2. During one collision event, either one or the other or both particles can have a wet spot on the colliding surface,

$$\eta_{coll} = 2\frac{A_{drop,base}}{A_{p,surf}} = 2\frac{a_{drop}^2}{d_{pp}^2} \approx \frac{N_{coll,wet}}{N_{coll}} \tag{30}$$

η_{coll} also takes into account wet-wet collisions which are especially relevant when the dissipation of energy by the liquid film is considered. This situation is favorable to prevent particles from rebounding and supports desired aggregation

Table 4. Simulation Test Cases

Case	Droplet Addition	Aggregation Occurrence
A	One droplet per particle at $t = 0$	No aggregation
B	No addition of binder	Every dry collision
C	Continuous	No aggregation
D	Continuous	Every wet collision

Droplets are assumed to maintain their semielliptical shape after deposition. Predrying during flight and drying of deposited droplets are neglected.

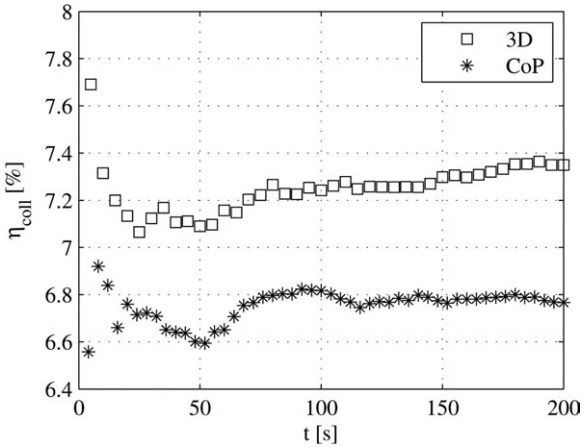

Figure 10. Collision efficiencies for Case A simulated by the extended CoP and the 3-D structure algorithm.

The 3-D algorithm predicts the collision efficiency according to the surface coverage by a single droplet. In the CoP algorithm, the number of droplet positions has to be integer and needs to be rounded. Thus, the size of the wet surface area is underestimated, leading to smaller (or eventually larger) collision efficiencies.

events. Figure 10 compares the collision efficiencies of the extended CoP with the 3-D structure algorithm. In our concrete case, a single droplet covers 3.67% of a primary particle's surface. Thus, we are expecting a collision efficiency of around 7.33%, which is precisely met by the 3-D algorithm. Because of rounding, the CoP algorithm assumes five droplet positions per sector, adding up to 30 positions per particle ($K_{max} = 6$), whereas the accurate value is 27.28 positions. This deviation leads to a droplet surface coverage by a single droplet which is virtually reduced to 3.33% or an expected collision efficiency of 6.66% (instead of 7.33%). After 200 s the expected values are met by both algorithms.

The length of process time equals ~200,000 binary collisions here. Because of the stochastic nature of the process, every simulation needs to be run repeatedly to reach statistical accuracy. Figure 11 shows the oscillation of curves following the CoP just by repeating the same scenario five times. In contrast to that, deterministic calculations evolve continuously in time and will reproduce exactly the same result over and over again.

Case B: every collision leads to aggregation

In the purely theoretical Case B, we assume a dry fluidization of particles. Although no binder is added to the powder bed, every collision is assumed to lead to a successful aggregation event. Case B is one of two benchmarking cases regarding the efficiency of the process: either every collision equals an aggregation or every droplet introduced to the fluid bed forms a binder bridge. In reality, agglomeration rates will be much slower than predicted by these two cases. The maximum collision efficiency corresponds to a very fast reduction of the number of particles. Depending on the collision rate, the total particle number in the real system will exponentially tend to one. This situation is expressed by the differential equation 11 and its analytical solution, Eq. 12. To obtain the actual particle number of the real system from the simulation box, we calculate the average mass of a single particle in the simulation box $M_{p,MC}$. The average

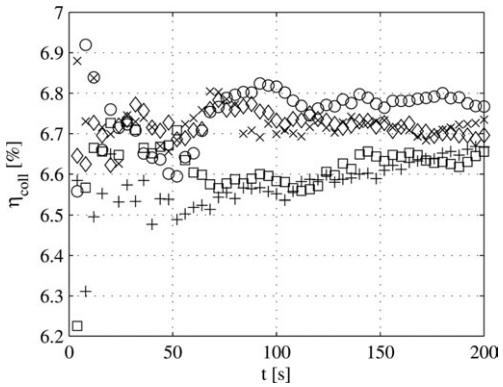

Figure 11. Collision efficiency calculated by the repeated application of the CoP algorithm under equal conditions for Case A.

The results of any stochastic simulation algorithm vary in a certain range. Thus, one needs to perform every simulation several times and average the outcome to increase accuracy and reliability.

particle mass is an intensive property and, thus, equivalent in the simulation box and the real system. While the particle number in the simulation box remains constant, the particle number in the real system can be expressed as

$$N_{\mathrm{p}}(t) = \frac{M_{\mathrm{bed}}}{M_{\mathrm{p,MC}}(t)} \tag{31}$$

The total bed mass M_{bed} is considered constant throughout the process, neglecting the eventual addition of binder mass. Figure 12 shows the decrease of particle number in the real system relative to the initial particle number. Both algorithms, CoP and 3-D, show satisfactory accordance with the analytical solution, which is a measure of correctness for the time discretization within the algorithm.

Case B is a very good test to prove the accuracy of time discretization. The time-continuous analytical solution only includes the collision frequency (Eq. 12), physical phenomena of the process are not taken into consideration. As long as the collision frequency is simply a constant value, this maximum aggregation rate has to be met by every algorithm. Minor deviations result from the fact that the continuous solution also considers nondiscrete particle numbers in the process. In the present work, the particle number is adjusted after every collision to keep the simulated number constant during the process. Thus, the collision frequency in the simulation box $f_{\mathrm{coll,MC}}$ remains constant (see Eq. 3). The algorithm presented by Terrazas-Velarde et al.[5] follows a different approach. In Figure 5, which is similar to Figure 12, we notice a relatively large deviation to the analytical solution. In their constant-volume algorithm, the simulation particle number, and consequently the collision frequency $f_{\mathrm{coll,MC}}$, is only regulated when the initial particle population has been doubled or reduced by 50%.

Case C: continuous addition of liquid, no aggregation

In Case C, the binder liquid is added continuously with a constant rate. This is comparable to a real process scenario. Similarly to Case A, we will count wet collisions, but completely switch off aggregation. This assumption will keep the initial particle number constant throughout the whole process, only the mean wet surface fraction of single particles will increase with time. Figure 13 shows the collision efficiency calculated by the 3-D algorithm and the extended CoP. Both simulation algorithms stay below the theoretical limit of Eq. 30, which assumes an instantaneous usage of binder droplets as soon as they are introduced into the system. As discussed in Case A, the CoP underestimates the collision success. The wetted particle surface fraction is virtually smaller than the real one due to roundings of the discrete number of positions. The collision efficiency increases linearly with time, as the number of droplets in the system also does.

As depicted in Figure 10 for the artificial situation of one droplet per particle, the theoretical collision efficiency is reached only after a certain amount of time. In Case C, we permanently add droplets so that we never reach the theoretical equilibrium value, which assumes an instantaneous usage of every deposited droplet. To clarify this situation, we performed the following simulation experiment: after 20 s of process time, the binder spray was stopped. This equals an amount of 1000 (continuously added) droplets in the simulation box and a surface coverage of, again, 7.33% (compare with Case A). The particles keep colliding after that. As depicted in Figure 14, the theoretical limit increases linearly in the first 20 s, corresponding to the continuous addition of droplets. After 20 s the theoretical limit remains constant, while the collision efficiency calculated by the 3-D algorithm converges to it. After about 180 s the 3-D collision efficiency remains constant. The time to reach this asymptote, or the theoretical collision efficiency, directly correlates with the collision frequency. Here, we have applied a value of two collisions per particle and second, which is relatively low. For collision frequencies tending to infinity, the simulation would exactly and instantaneously meet the theoretical limit.

Furthermore, droplets are deposited on randomly chosen particles leading to a heterogeneous binder distribution on the particles. This situation differs from Case A, where exactly one droplet was placed per particle. In the actual Case C, some particles may contain two or more droplets, whereas others will carry no droplet at all. With increasing number of droplets per particle in the 3-D algorithm, droplets will start to overlap and, thus, the covered surface area of the particle will be reduced. Even though the effect is

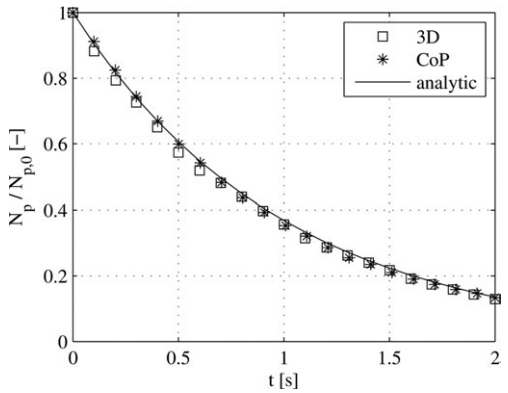

Figure 12. Particle number decrease in the real system for Case B (maximum aggregation rate).

Extended CoP (asterisks) and 3-D structure algorithm (squares) both follow the analytical solution, which is a measure of correctness for the time discretization within the algorithm. Only short simulation times such as 2 s can be applied, because the process is very fast and the number of primary particles in the simulation box increases exponentially with time.

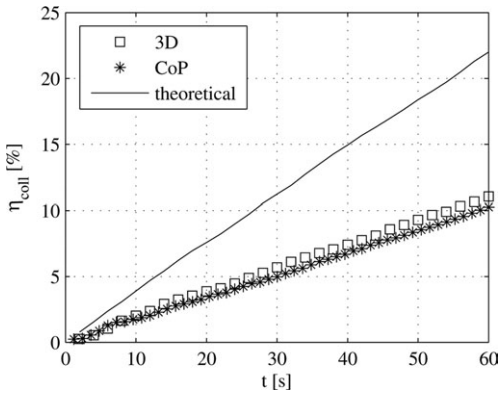

Figure 13. Wet collisions per total number of collisions in the simulated system for Case C.

The number of droplets in the system increases linearly so that there is no steady-state collision efficiency to be reached.

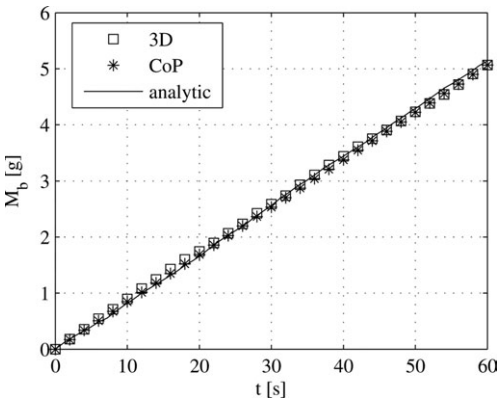

Figure 15. Sprayed binder mass in the real system (Case C).

CoP and 3-D algorithms meet the droplet spray rate even though addition time steps vary stochastically. The process time of 60 s refers to ~3000 droplets added to the simulation box.

small, it can be quantified by the simulation reaching asymptotically only 6.9% in Figure 14, whereas the maximal theoretical value is 7.33%, as discussed in Case A. Thus, the overlapping of droplets causes a reduction of wetted surface area and, consequently, a reduction of collision efficiency. In the CoP overlapping of droplets is not possible.

The simulated spray rate is checked by the cumulated amount of binder in the system vs. time, depicted in Figure 15. The analytical solution is simply the spraying rate multiplied by process time

$$M_{b,theoretical} = \dot{V}_b \rho_b t \tag{32}$$

In contrast to Terrazas-Velarde et al.,[5] who add a droplet whenever the process time reaches the droplet addition time, the droplet addition time has not a constant value in the here presented algorithms. In both the extended CoP and the 3-D structure algorithm, droplet addition is a stochastic event similar to the collision of particles. This means, that the time step after which a droplet is added is exponentially distributed, and the probability of occurrence correlates with the rate $\dot{N}_{drop}$. The use of a normal droplet size distribution would induce stronger oscillations of the amount of binder in the system around the theoretical value. For the present situation of equally sized droplets, the deviation is caused only by the varying length of time steps. Such deviations are small so that the agreement between simulations and theoretical solution is very good.

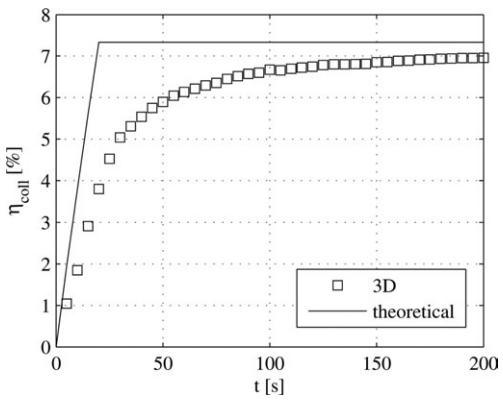

Figure 14. Modified Case C (cf. Figure 13): after 1000 droplets, had been introduced into the simulation box (~20 s process time), the continuous addition of binder was stopped.

It takes about 180 s for the simulation to asymptotically approach a constant value. The simulated collision efficiency does not increase further than 6.9% due to the nonuniform distribution of droplets on the particles leading to overlapping. This effect virtually decreases the wetted surface area and, consequently, the collision efficiency. In the CoP, overlapping of droplets is not possible.

Case D: structural evolution of particles and sterical accessibility of binder

Simulation Case D includes the continuous addition of binder to the simulation box. An interparticle collision will result in aggregation when a wet spot of the surface of either one or both particles is hit during the binary collision. Case D may be considered as the most realistic of our theoretical verification, even though we still neglect predrying and the drying of deposited droplets. The extended CoP and the novel spatial structure algorithm both predict similar growth behavior of particles, (Figure 16). After only 50 s of process time, we have less than 10% of the initial number of particles in the process chamber. As breakage is not considered here, size enlargement dominates the system. Theoretically, after infinite process time, all initial primary particles will be joined together to form one single agglomerate. Typical for fluidized bed agglomeration, we notice three different periods during the process. First, the particle number in the fluidized bed decreases relatively slowly. In this period, which corresponds in Figure 16 to the first 10 s of the process, mainly primary particles aggregate. Within the next 30 s cluster-cluster aggregation occurs, and the total particle number drops massively. At the end of the depicted time span, the number reduction rate decreases again, as the particle number in the process is already quite low. From now on, the relative particle number will asymptotically approach zero. Depicted in Figure 16 are also the theoretical limits to the number reduction for the case that every collision equals an aggregation (maximum collision) and for the case that every droplet can be used for aggregation (maximum droplet). These benchmarking limits correspond to Cases B and C of our validation, respectively. As mentioned earlier, real aggregation rates will be much slower.

As aggregates integrate more and more primary particles in their structure, they change sterically. One droplet per

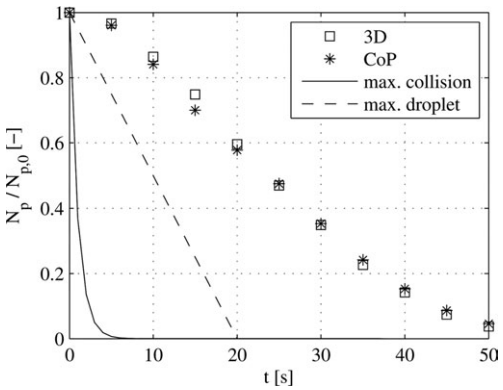

Figure 16. Relative number reduction of particles for simulation case D.

Maximum collision (Case B) and maximum droplet (Case C) refer to the benchmarking situations of every collision event or every droplet added to the simulation box leading to aggregation.

binder bridge is used to connect two primary particles with each other. Free droplets – although they do not dry in this theoretical consideration – may become deactivated by neighboring particles. Figure 17 depicts such a particle structure calculated by the 3D algorithm, containing primary particles and deposited droplets.

The evolution of agglomerate structure is unrestricted in the algorithm, which assembles the primary particles according to the collision procedure. In the real process, consolidation may take place by rearrangement of peripheral primary particles into the inner structure. Such densification may be driven by collisions leading to breakage or attrition. Here, we do not consider breakage or any kind of reorganization of particle structure. Thus, predicted particles are rather loose and dendritic, as in Figure 17. To express the particle structure with a single parameter, the coordination number K is used. K measures the direct primary neighbors of every single primary particle within the structure. Terrazas-Velarde et al.[5] define a maximum coordination number of $K_{max} = 6$ for their CoP. Depending on the underlying model and the expected porosity of agglomerates, K_{max} can range from 6 (cubic grid) up to 12 (hexagonal densest packing) for aggregates formed by monodisperse primary particles. Every primary particle is forced to have between zero and K_{max} neighbors. Figure 18 depicts the mean and maximum coordination number of the spatial structure algorithm (left) and the extended CoP (right) vs. time. In agreement with the missing consolidation procedure, K_{mean} asymptotically reaches a relatively low value of $\sim$2 for both algorithms. This underlines the high particle porosity, which is a typical feature of agglomerates produced in fluidized beds. In comparison, drum or high-shear granulators generally create denser agglomerates.[25] After running the 3-D algorithm repeatedly, the maximum coordination number never exceeded a value of 6. In the beginning of the process, K_{max} is determined by the aggregation of single primary particles. In later stages of the process, already-complex agglomerates, which occupy large space, collide and cover wide regions of the collision partner. After 60 s of process time, the maximum and mean coordination number do not change anymore. For polydispersed primary particles, larger values of K_{max} are expected. The maximum coordination number calculated by the CoP algorithm is 6 in any case. This is somewhat trivial as K_{max} is one of the parameters that need to be given in advance to run the CoP-simulation. In the primary particle collision stage (first 20 s), the mean coordination number increases faster than the 3-D mean: particles attach primary particles in a more effective way. This agrees with Figure 16. During the early stage of the process, the CoP predicts a slightly higher aggregation rate, which might be due to the predefined structure of agglomerates.

Figure 19 shows the density distribution q_0 of the number of primary particles per agglomerate after a process time of 50 s. According to the 3-D algorithm, the most agglomerates contain less than 50 primary particles. Starting from monodispersed particles, the distribution broadens with time. The fraction of agglomerates containing between 100 and 150 primary constituents is very small. This fraction would be likely to break first in case of considering breakage in the algorithm. The distribution of Figure 19 corresponds to a very high degree of aggregation in the fluidized bed: the initial particle number was reduced to less than 10% (see also Figure 16). The density distribution calculated by the CoP algorithm is somewhat narrower, which supports the assumption that the particles are more compact. There are almost no aggregates containing more than 100 primary particles.

Finally, we compare the state of droplets in the 3-D algorithm and in the extended CoP. Although there are no underlying physical differences, the algorithm itself can create different kinetic effects. In Figure 20, we distinguish three different states of single droplets in the simulation box:

- a droplet may be completely accessible for colliding particles and, thus, active for bridge formation,
- it may be sterically hidden in the particle structure, meaning deactivated for bridge formation, or
- the droplet may have already been used for binder bridge formation.

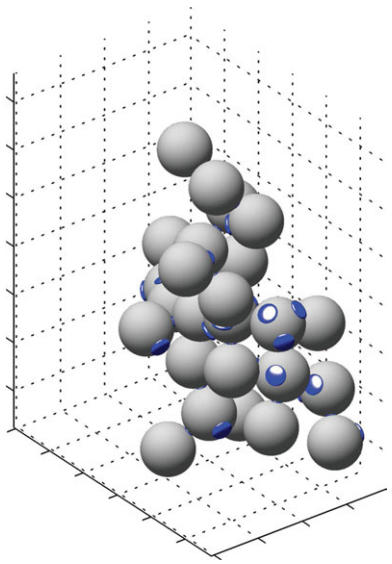

Figure 17. Agglomerate structure calculated by the 3-D algorithm containing primary particles and wet droplets.

Droplets situated inside the structure may be hidden by sterical effects of connected primary particles. This structural effect influences the kinetics of the process, as binder liquid is not necessarily used for aggregation.

[Color figure can be viewed in the online issue, which is available at wileyonlinelibrary.com.]

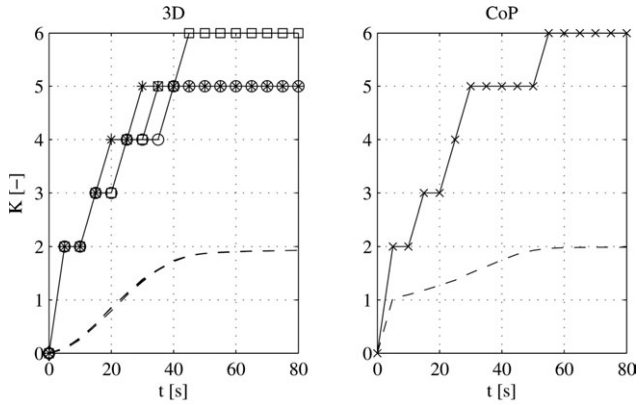

Figure 18. Maximum (solid lines with markers) and mean (broken curve) coordination number of primary particles in the simulation box, calculated by the 3-D (left) and the CoP (right) algorithm.

To sustain the fluidization of larger agglomerates, the gas mass flow rate was increased to 40 kg/h instead of 25 kg/h in the base case.

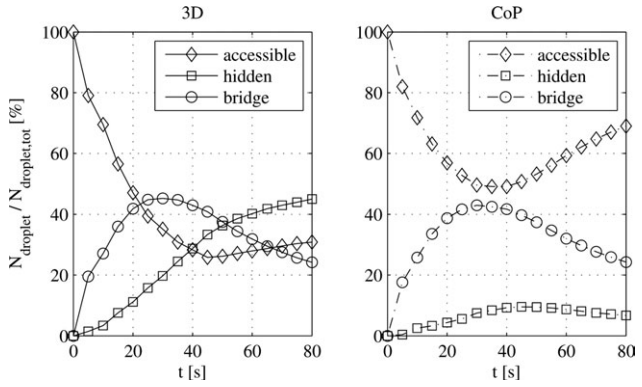

Figure 20. State of binder droplets in the simulation box without consideration of drying: used in binder bridges, accessible, or sterically hidden.

The total number of the different groups of droplets in the system increases steadily but with different slopes.

In the beginning of the process, the number of bridges increases rapidly in both algorithms. After 30 s of process time, the relative number of droplets used for bridge formation reaches its maximum before slowly dropping down again. This situation is similar for both algorithms. To explain why the relative number of droplets decreases after some point of time in both algorithms, two facts must be considered. First, the absolute number of bridges increases steadily during the process. Second, the total number of droplets in the system increases at a higher rate, consisting of the sprayed droplets and droplets located on copied particles. Even if we would stop spraying binder, the number of droplets in the system would still increase due to the substitution of aggregating particles performed to maintain the statistical accuracy. The substitution increases the size of the simulation box during the process so that the scaling factor S and the number of droplets entering the simulation box per unit time also increase (Eq. 2). By copying particles also "new" bridges appear, but this effect is small compared to the production of droplets. In both algorithms, the number of bridges is similar throughout the process, resulting in comparable growth of agglomerates, (Figures 16 and 19).

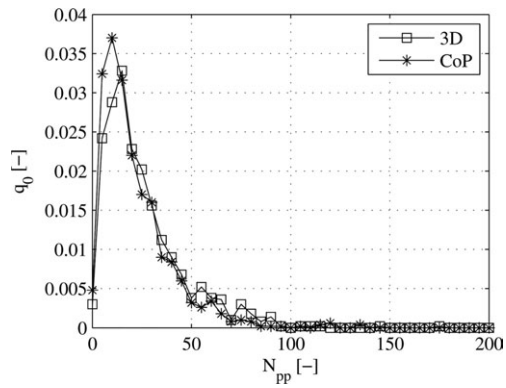

Figure 19. Density distribution q_0 of the number of primary particles per agglomerate.

The CoP distribution contains hardly any particles with more than 100 constituents. This is due to the nature of the CoP collision algorithm, which preserves a certain particle structure with given collision positions.

As long as the number of primary particles per aggregate is low, the hidden surface fraction per particle is small, and almost every droplet added to the powder bed is used for aggregation. However, this fraction becomes significant after about 10 s. From that point of time, the accessibility of not-yet-used droplets deviates strongly between the two algorithms. In the 3-D algorithm (left), the fraction of accessible droplets decreases to 30%, whereas the CoP (right) predicts about 70% of the total number of droplets in the system to be accessible for interparticle collisions. Simultaneously, the prediction of the fraction of sterically hidden binder droplets by the 3-D algorithm (up to 45%) differs significantly from the prediction of the same fraction of droplets in the CoP (10% maximum), even though the number of bridges is basically the same. In the following, we will attempt to explain why the fractions of sterically hidden and accessible droplets are so different for the two algorithms according to Figure 20.

In the extended CoP one sector on each of the two particles is blocked after a successful collision, (Figure 6). As $K_{max} = 6$, $1/K_{max} = 16.67\%$ of the particle surface is deactivated for further collisions. This means that the droplet positions contained by the specific sector cannot take up a fresh droplet anymore. The CoP algorithm does not take into account the additional sterical hinderance by other primary particles surrounding the collision spot. Consequently, the shielded particle surface area is relatively small. The 3-D algorithm shows two main differences. First, the surface shielded within a complex particle structure is much larger than predicted by the CoP. This effect is schematically illustrated in Figure 21. Although the inner space of the example aggregate is sterically hidden for further collision contacts in reality, the CoP would allow primary particles to attach to the cavity. The 3-D algorithm considers the full geometrical structure of the particle and is, thus, physically more reasonable. While a complete sector and all its droplet positions are blocked for future interaction with particles or droplets in the CoP, the sterically hidden surface of the 3-D particle in Figure 21 can still host a droplet as this can pass into the cavity. Such a droplet would be deactivated for aggregation

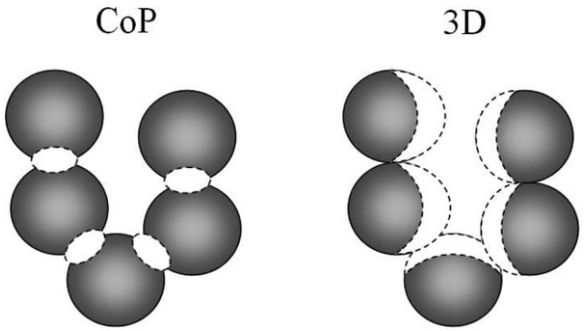

Figure 21. Illustration of the treatment of a particle in CoP (left) and 3-D (right).

After successful collision, a small surface area corresponding to one sector per particle is sterically shaded in the CoP algorithm (white spots next to particle contacts). In the spatial structure, evolving from the 3-D algorithm, much more surface area is impeded by surrounding primary particles.

from the very first moment of deposition. Hence, there is a distinction between droplet deposition and particle contact in 3-D, whereas the CoP either allows a surface to be accessible to both droplets and particles or to none of them. Moreover, the first droplet deposited on a CoP particle is never sterically hidden. This is the second significant difference between the two compared algorithms.

Figure 22 shows that the minimum surface coverage by a particle contact assumed by the CoP is realistic only for straight particle chains. As soon as agglomerate structures deviate from this configuration, the sterical effect is not covered in a correct way.

To further elaborate the different treatment of sterical effects in the two algorithms, the accessible surface area was calculated for aggregates containing different number of primary particles. Results are presented in Table 5. For a single particle, we obtain the trivial fact that 100% of the surface area is accessible. A second primary particle decreases this value by 16.7% in the CoP. Additional primary particles cause a further decrease, which is moderate in the CoP because the algorithm does not take into account the presence of surrounding primary particles. The accessible surface fraction predicted by the CoP is deterministic, depending only on the number of primary particles. The shielded surface area of agglomerates simulated in 3-D depends on the individual structure and varies stochastically for more than two primary particles. However, it is always much larger than in the CoP.

As explained, one can follow these characteristics also in Figure 20. The CoP predicts only a small amount of sterically hidden droplets throughout the simulation. The values

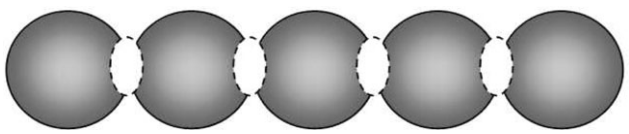

Figure 22. In the extended CoP, the particle surface accessible for interparticle collisions is reduced by a constant fraction $1/K_{max}$ after every successful aggregation event.

The white spots are sectors deactivated for droplet collision in the CoP, though they are still large enough to host a droplet coming vertically from top or bottom. This would be possible in the 3-D algorithm.

Table 5. Accessible Fraction of Agglomerate Surface for Different Numbers of Primary Particles

N_{pp}	$A_{surf,free}$ (%)	$A_{surf,free}$ (%)
	3-D	CoP
1	100.0	100.0
2	74.2	83.3
3	65.5	77.8
4	61.1	75.0
5	52.4	73.3
6	52.9	72.2
7	48.5	71.4

According to the CoP algorithm, only the regions around primary particle contacts are sterically hidden. Thus, the covered surface fraction is small (only 16.7% per primary particle and bond).

increase after the initial stage of primary particle collisions and attain a maximum of around 10%. The fraction of accessible droplets evolves accordingly. After 80 s of process, 70% of the droplets introduced to the simulation box are active for aggregation. The 3-D algorithm shows a different behavior: much more droplets are impeded in the particle structure. As the number of bridges is similar in both algorithms, a smaller number of accessible droplets are used much more efficiently in 3-D than a higher number of accessible droplets in the CoP. It should be stressed that the CoP is a mathematical approach to express certain particle properties. A geometrical reconstruction in terms of particle structure is outside of the scope the CoP, so that sterical effects are not captured in a satisfactory way.

Conclusions

This article presented a Monte Carlo model to simulate the particle formation in fluidized bed agglomeration processes. The modeling method, which is based on the temporal evolution of a discrete particle sample influenced by various microprocesses, was briefly discussed. Two important aspects are the correlation with real time and the simulation box size. The agglomeration process was treated as a memoryless Markov process,[17] and event frequencies were defined for droplet addition and interparticle collisions. The simulation box contains 1000 particles, considered to be representative for the global process. Two different model approaches were compared. First, a novel 3-D structure algorithm, which develops a spatial particle structure during the process, was presented. Second, a previous approach[5,14,15] which simplifies the particle structure using the CoP was extended. Different particle morphologies obtained by the two algorithms were discussed by droplet state and coordination number. By applying four different test cases, both models were theoretically verified and their accuracy and behavior were checked by comparison to simple analytical solutions. Droplet drying and particle breakage were not considered here.

The 3-D simulation algorithm and the CoP both agree with expected collision efficiencies (Case A) and maximum aggregation rates (Case B). Furthermore, the binder addition rate of the real process is accurately predicted, even though the event droplet addition is randomly distributed throughout the stochastic simulation. It can, thus, be concluded that both approaches represent the physical process correctly.

The main differences between the two algorithms lie in the predicted particle morphology and the simulation speed. The CPU times for calculating Case D with different simulation box sizes are given in Table 6. The simulation particle number exponentially scales the simulation time. For low

Table 6. CPU Performance of 3-D and CoP Algorithm Under Variation of the Particle Number in the Simulation Box (Intel Core 2 Duo, 1.8 GHz)

Particle Number	CPU Time CoP (s)	CPU Time 3 D (s)
100	4	20
200	15	102
500	81	384
1000	294	1482

Process and simulation parameters are adapted from Case D. Real time to be simulated was 50 s.

particle numbers, the statistical representativeness of the sample decreases, but the simulation is very fast. The CoP mathematically assembles information in matrices, which is very effective from a computational point of view. In any case, the CPU speed is four to five times faster than for the more complex 3-D algorithm. As results for the investigated theoretical test cases are comparable, the CoP can be regarded as a good and fast estimation method.

A big advantage of the novel 3-D algorithm is, however, seen in the unrestricted and physically justified development of particle structure. The 3-D simulation algorithm preserves and updates the complete history of every particle and droplet entering the simulation box. It can, therefore, be easily extended to account for drying and the increase of solute concentration in deposited droplets with time in future works. The same holds for droplet penetration in porous primary particles. By separating the active—wet and accessible—binding agent on the particle from the already used or sterically hidden fraction inside the aggregate structure, the 3-D algorithm will certainly facilitate the derivation of new and more realistic kinetic expressions for population balances. It should be noted that the CoP is not able to handle distributions of droplet and primary particle sizes. Overlapping of droplets is not considered, and a certain particle structure is intrinsically implied in the CoP algorithm. The individual state of a droplet or particle colliding with another particle of distributed size can only be captured by the spatial algorithm which takes into full account the effect of neighboring particles.

The here presented analysis was algorithmic, aiming at the evaluation of merits and disadvantages of the two investigated Monte Carlo approaches by comparison, and at their verification for simple limiting cases. Validation was only indirect, from the previous comparison on a CoP algorithm with experimental results.[14,15] Therefore, the direct experimental validation of the 3-D algorithm will be in the focus of future work. To this purpose, droplet predrying before deposition leading to eventual overspray, drying of deposited droplets, and particle breakage will be included in the model. The Stokes concept will extend the collision algorithm to decide, whether a liquid film is able to dissipate the kinetic energy of collision impact or not, rather than assuming every wet collision to be successful. Breakage and fragmentation will contribute to more compact particles and reduced primary particle numbers per agglomerate. The latter limits the upper system size, with positive consequences for the simulation time. Additionally to macroscopic process results, such as particle size or moisture content, it is planned to compare structural information of single particles, for example coordination numbers, with scanning electron microscopy and x-ray tomography data to further elaborate the microprocess level.

Acknowledgments

The authors gratefully acknowledge the funding of this work by the German Federal Ministry of Education and Research (BMBF) as part of the InnoProfile project NaWiTec.

Literature Cited

1. Ramkrishna D. The status of population balances. *Rev Chem Eng*. 1985;3:49–95.
2. Litster JD. Scaleup of wet granulation processes: science not art. *Powder Technol*. 2003;130:35–40.
3. Peglow M, Kumar J, Heinrich S, Warnecke G, Tsotsas E, Mrl L, Wolf B. A generic population balance model for simultaneous agglomeration and drying in fluidized beds. *Chem Eng Sci*. 2007;62:513–532.
4. Smith M, Matsoukas T. Constant-number Monte Carlo simulation of population balances. *Chem Eng Sci*. 1998;53:1777–1786.
5. Terrazas-Velarde K, Peglow M, Tsotsas E. Stochastic simulation of agglomerate formation in fluidized bed spray drying: a micro-scale approach. *Chem Eng Sci*. 2009;64:2631–2643.
6. Maisels A, Kruis FE, Fissan H. Direct simulation Monte Carlo for simultaneous nucleation, coagulation, and surface growth in dispersed systems. *Chem Eng Sci*. 2004;59:2231–2239.
7. Tan H, Salman A, Hounslow M. Kinetics of fluidised bed melt granulation, Part I: The effect of process variables. *Chem Eng Sci*. 2006;61:1585–1601.
8. Garcia AL, van den Broeck C, Aertens M, Serneels R. A Monte Carlo simulation of coagulation. *Physica A*. 1987;143:535–546.
9. Liffmann K. A direct-simulation Monte-Carlo method for cluster coagulation. *J Comuput Phys*. 1992;100:116–127.
10. Park H, Kim S, Chang H. Brownian dynamic simulations for the aggregation of charged particles. *J Aerosol Sci*. 2001;32:1369–1388.
11. Kruis FE, Maisels A, Fissan H. Direct Simulation Monte Carlo Method for Particle Coagulation and Aggregation. *AIChE J*. 2000;46:1735–1742.
12. Fries L, Antonyuk S, Heinrich S, Palzer S. DEM-CFD modeling of a fluidized bed spray granulator. *Chem Eng Sci*. 2011;66:2340–2355.
13. Maronga SJ, Wnukowski P. Modelling of the three-domain fluidized-bed particulate coating process. *Chem Eng Sci*. 1997;52:2915–2925.
14. Terrazas-Velarde K, Peglow M, Tsotsas E. Kinetics of fluidized bed spray agglomeration for compact and porous particles. *Chem Eng Sci*. 2011;66:1866–1878.
15. Terrazas-Velarde K, Peglow M, Tsotsas E. Investigation of the kinetics of fluidized bed spray agglomeration based on stochastic methods. *AIChE J*. 2011;57:3012–3026.
16. Zhao H, Maisels A, Matsoukas T, Zheng C. Analysis of four Monte Carlo methods for the solution of population balances in dispersed systems. *Powder Technol*. 2007;173:38–50.
17. Gillespie DT. A general method for numerically simulating the stochastic time evolution of coupled chemical reactions. *J Comput Phys*. 1976;22:403–434.
18. Buffière P, Moletta R. Collision frequency and collisional particle pressure in three-phase fluidized beds. *Chem Eng Sci*. 2000;55:5555–5563.
19. Oesterle B, Petitjean A. Simulation of particle-to-particle interactions in gas solid flows. *Int J Multiphase Flow*. 1993;19:199–211.
20. Reuter K. *Modeling Heterogeneous Catalytic Reactions: From the Molecular Process to the Technical System*. Weinberg: Wiley-VCH, 2009.
21. Ennis BJ, Tardos G, Pfeffer R. A microlevel-based characterization of granulation phenomena. *Powder Technol*. 1991;65:257–272.
22. Stepánek F, Rajniak P, Mancinelli C, Chern R, Ramachandran R. Distribution and accessibility of binder in wet granules. *Powder Technol*. 2009;189:376–384.
23. Leba H, Cameirao A, Herri JM, Darbouret M, Peytavy JL, Glnat P. Chord length distributions measurements during crystallization and agglomeration of gas hydrate in a water-in-oil emulsion: simulation and experimentation. *Chem Eng Sci*. 2010;65:1185–1200.
24. Meric RA, Erbil HY. Evaporation of Sessile Drops on Solid Surfaces: pseudospherical Cap Geometry. *Langmuir*. 1998;14:1915–1920.
25. Hogekamp S, Pohl M. Porosity measurement of fragile agglomerates. *Powder Technol*. 2003;130:385–392.

Manuscript received July 19, 2011, revision received Sept. 23, 2011, and final revision received Nov. 22, 2011.